Bidirectional coupling between integrin-mediated signaling and actomyosin mechanics explains matrix-dependent intermittency of leading-edge motility

Erik S. Welf, Heath E. Johnson, and Jason M. Haugh
Department of Chemical and Biomolecular Engineering, North Carolina State University, Raleigh, NC 27695

ABSTRACT **Animal cell migration is a complex process characterized by the coupling of adhesion, cytoskeletal, and signaling dynamics. Here we model local protrusion of the cell edge as a function of the load-bearing properties of integrin-based adhesions, actin polymerization fostered by adhesion-mediated signaling, and mechanosensitive activation of RhoA that promotes myosin II–generated stress on the lamellipodial F-actin network. Analysis of stochastic model simulations illustrates how these pleiotropic functions of nascent adhesions may be integrated to govern temporal persistence and frequency of protrusions. The simulations give mechanistic insight into the documented effects of extracellular matrix density and myosin abundance, and they show characteristic, nonnormal distributions of protrusion duration times that are similar to those extracted from live-cell imaging experiments. Analysis of the model further predicts relationships between measurable quantities that reflect the partitioning of stress between tension on F-actin–bound adhesions, which act as a molecular clutch, and dissipation by retrograde F-actin flow.**

Monitoring Editor
Alex Mogilner
University of California, Davis

Received: Jun 10, 2013
Revised: Sep 9, 2013
Accepted: Oct 15, 2013

INTRODUCTION

Cell migration is an essential process in embryonic development, wound repair, and both innate and adaptive immune responses. Movement of epithelial and mesenchymal cells is marked by the rich dynamics of the actin cytoskeleton responsible for force generation, the adhesion complexes responsible for force transduction, and the biochemical regulatory networks responsible for signal transduction (Parsons *et al.*, 2010). Orchestrating these dynamics are integrins, transmembrane adhesion receptors that engage both the actin cytoskeleton and the extracellular matrix (ECM) to transfer force during cell migration (Gardel *et al.*, 2010; Huttenlocher and Horwitz, 2011; Boettiger, 2012). In addition to acting as mechanical linkages, integrins cluster into discrete complexes that recruit numerous intracellular signaling proteins, which modulate polymerization of actin filaments and activation of the motor protein myosin II; small GTPases of the Rho family, such as Rac, Cdc42, and RhoA, are especially important in integrin-mediated signaling (Ridley *et al.*, 2003). Polymerization of the F-actin network is associated with protrusion of the leading membrane edge and, ultimately, cell translocation, whereas myosin II cross-links F-actin some distance away from the leading edge and mediates contraction. Contractility of the actomyosin network serves to move the cell body forward but also reins in protrusion by imposing a rearward stress on the actin network (Vicente-Manzanares *et al.*, 2009b).

It has been appreciated for some time that actin, adhesion, and signaling dynamics are spatially and temporally integrated, and that this integration is both mechanical and biochemical in nature (Lauffenburger and Horwitz, 1996; Sheetz *et al.*, 1998). In support of this concept, a preponderance of evidence indicate that protrusion is coupled to formation of nascent adhesions (Choi *et al.*, 2008), nascent adhesions promote actin polymerization through activation of Rac and other signaling pathways (Nayal *et al.*, 2006), physical linkage between adhesion complexes and F-actin constitutes a mechanical clutch that is required for productive protrusion instead of retrograde flow (Ji *et al.*, 2008; Vicente-Manzanares *et al.*, 2009a;

This article was published online ahead of print in MBoC in Press (http://www.molbiolcell.org/cgi/doi/10.1091/mbc.E13-06-0311) on October 23, 2013.
Address correspondence to: Jason M. Haugh (jason_haugh@ncsu.edu).
Abbreviations used: ECM, extracellular matrix; GFP, green fluorescent protein.

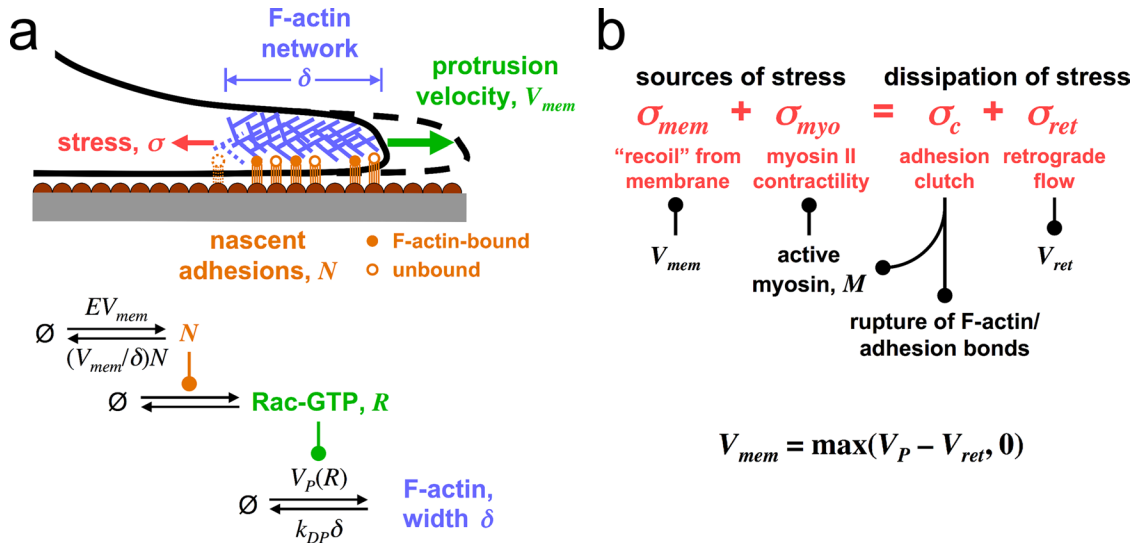

FIGURE 1: Physicochemical model of leading-edge protrusion. (a) Adhesion dynamics and signaling. Nascent adhesions, which are either uncoupled (open circle) or coupled (filled circle) to the F-actin network of the lamellipodium, form at a rate proportional to the velocity of membrane protrusion, V_{mem}, depending on an efficiency parameter, E, that is related to ECM density. Nascent adhesions turn over as they emerge from the back of the F-actin network; the frequency of turnover is determined by V_{mem} and the F-actin network width, δ. Activation of Rac signaling, which stimulates local actin polymerization and accordingly augments δ, is mediated by nascent adhesions. (b) Stress balance on the F-actin network. Stresses exerted on the actin network by myosin contractility and resistance of the membrane to deflection determine retrograde flow, in concert with the molecular clutch that mechanically links nascent adhesions and the F-actin network. The adhesion clutch determines how much of the stress is transferred to nascent adhesions; this stress affects the rupture of nascent adhesion/F-actin bonds and the mechanosensitive activation of myosin II.

Schwarz and Gardel, 2012), and adhesion complexes under tension promote activation of RhoA and myosin II (Riveline *et al.*, 2001; Guilluy *et al.*, 2011). These and other experimental breakthroughs, alongside innovations in live-cell fluorescence microscopy and image processing, have led to a call for more quantitative and mechanistically integrative analyses of cell migration (Danuser, 2011; Welf and Haugh, 2011; Hughes-Alford and Lauffenburger, 2012).

To develop insight into how interactions between the multiple molecular mechanisms just described produce the motility phenomena observed in mammalian cells, mathematical modeling has proven to be a valuable approach that complements the increasing complexity of the experimental data sets being acquired (Carlsson and Sept, 2008; Mogilner, 2009; Welf and Haugh, 2011). To be most effective, it is clear that quantitative models must be formulated based on sound chemical and physical principles, with due consideration of biological detail weighed against the need to specify adjustable model parameters.

Toward this end, we have constructed and analyzed a physicochemical model with the following characteristics. First, our focus here is on the cell's leading edge, capturing the dynamics of the branched F-actin network and nascent adhesion formation zone marking the lamellipodium (Ponti *et al.*, 2004; Small and Resch, 2005); although large static focal adhesions exist in the lamellum, where proportionally greater traction forces have been observed (Gardel *et al.*, 2008), we focus here on the more dynamic nascent adhesions due to their role in the signaling events that encourage actin polymerization and local protrusion (Nayal *et al.*, 2006; Choi *et al.*, 2008; Lee *et al.*, 2013). Phenomenological models cast at the level of a whole migrating cell (DiMilla *et al.*, 1991; Zaman *et al.*, 2005; Satulovsky *et al.*, 2008) have proven to be insightful, but a whole-cell model replete with mechanistic detail is not yet tractable. Second, our model merges what we consider the essential features of, and coupling between, cytoskeletal mechanics and intracellular signal transduction, which have been explored separately in models emphasizing either the mechanics (Rubinstein *et al.*, 2005, 2009; Wolgemuth, 2005; Enculescu *et al.*, 2010; Walcott and Sun, 2010; Zimmermann *et al.*, 2010; Barnhart *et al.*, 2011; Shemesh *et al.*, 2012) or biochemical aspects (Ditlev *et al.*, 2009; Cirit *et al.*, 2010; Welf and Haugh, 2010; Xiong *et al.*, 2010; Hu and Papoian, 2011; Maree *et al.*, 2012). Third, we implement the model as a stochastic simulation to capture the inherent fluctuations in lamellipodial network width (Giannone *et al.*, 2007) and in leading-edge protrusion velocity (Machacek and Danuser, 2006; Ryan *et al.*, 2012; Tsai and Meyer, 2012); the lack of an observable steady-state condition precludes a deterministic, continuum description as implemented in other models (Ditlev *et al.*, 2009; Barnhart *et al.*, 2011; Shao *et al.*, 2012). Finally, our analysis of the model is based on variation of conditions that have been manipulated experimentally, namely the density of surface-bound ECM (Palecek *et al.*, 1997; Gupton and Waterman-Storer, 2006; Cirit *et al.*, 2010) and manipulation of myosin II abundance or activity (Gupton and Waterman-Storer, 2006; Vicente-Manzanares *et al.*, 2007; Kuo *et al.*, 2011; Wolfenson *et al.*, 2011).

RESULTS

Formulation of a stochastic model coupling biochemical signaling and mechanical aspects of leading-edge adhesion and protrusion dynamics

We introduce here the ingredients and basic assumptions of the model (Figure 1). The protrusion engine is the lamellipodium, which contains a network of branched F-actin linked to the underlying substrate by nascent adhesions. The model tracks the width of the network, which changes according to the rates of actin polymerization at the front and depolymerization at the rear of

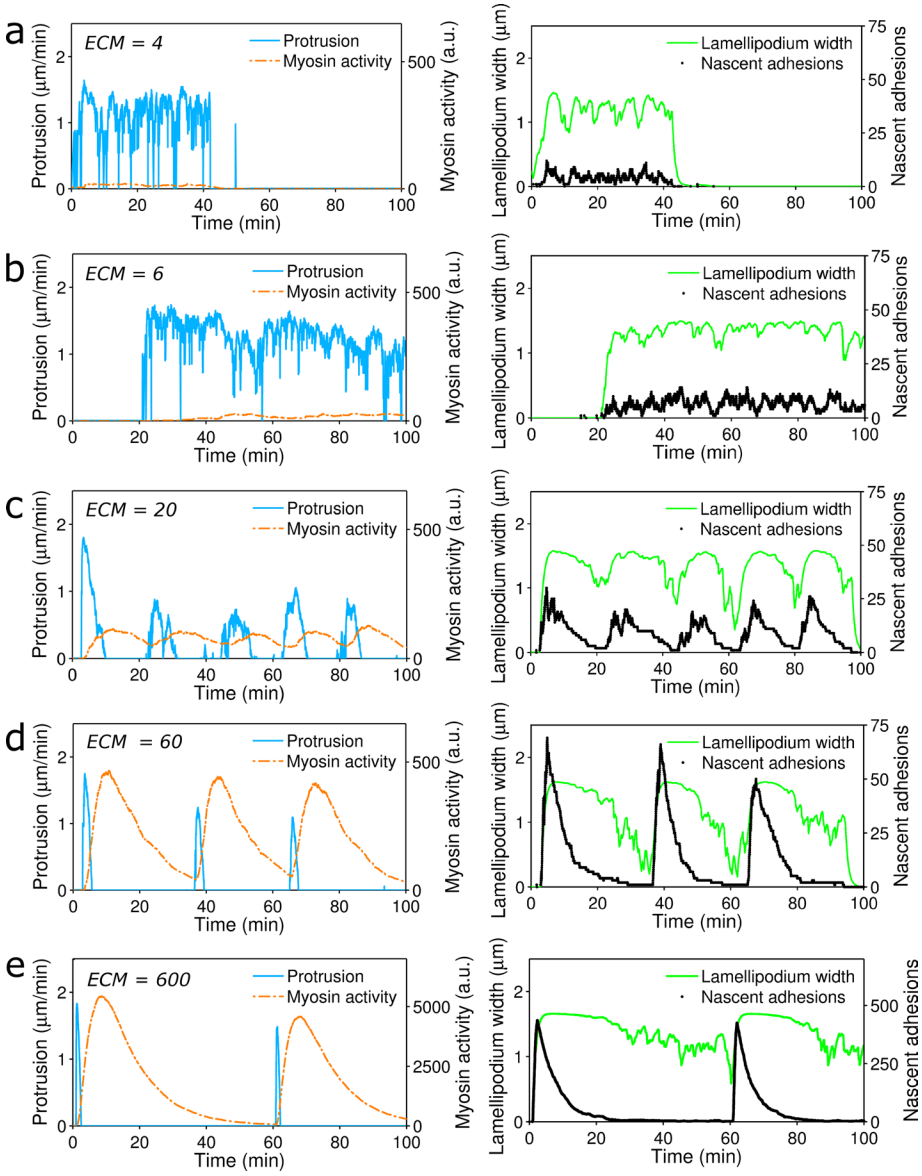

FIGURE 2: Stochastic simulations of protrusion dynamics as a function of ECM density. (a–e) Simulation output for a local patch of the lamellipodium, with different values of the ECM density parameter, E (μm^{-1}), as indicated. In each panel, membrane protrusion velocity (V_{mem}) and myosin activity (M) are shown in one plot, and lamellipodial width (δ) and nascent adhesion number (N) are shown in the other.

the lamellipodium. Nascent adhesion complexes have two distinct roles in promoting leading-edge protrusion (Figure 1a). The first is a signaling function, in which adhesions mediate the activation of Rac (as a proxy for a combination of signaling proteins), which in turn increases the rate of actin polymerization (Cox *et al.*, 2001; Nayal *et al.*, 2006). The second is a mechanical function, by which the adhesions bind reversibly to the F-actin network and thus serve as physical anchors to the underlying substratum. These interactions constitute a molecular clutch that allows slippage between adhesions and the actin network (Chan and Odde, 2008; Macdonald *et al.*, 2008). The clutch mechanism opposes a portion of the stress on the F-actin network as it polymerizes and thus allows translocation of the membrane boundary (Brown *et al.*, 2006; Hu *et al.*, 2007; Ji *et al.*, 2008). Nascent adhesions thus encourage productive membrane protrusion, and protrusion influences adhesion formation and turnover (Alexandrova *et al.*, 2008; Choi *et al.*, 2008), completing a positive feedback loop (Figure 1a).

Besides the more explicit inclusion of the adhesion-based clutch mechanism, the present framework improves upon our previous models (Cirit *et al.*, 2010; Welf and Haugh, 2010) in two fundamental ways, both of which reflect the mechanical nature of protrusion regulation (Figure 1b). The first is that the F-actin–bound adhesions are under tension and therefore mediate activation of myosin II. This mechanism is derived from evidence indicating that adhesion-based activation of the Rho/ROCK pathway is mechanosensitive (Guilluy *et al.*, 2011). Thus tension stimulates Rho signaling and activation of myosin II, which exerts contractile stress at the rear of the lamellipodium (Henson *et al.*, 1999; Brown and Bridgman, 2003; Jurado *et al.*, 2005; Cai *et al.*, 2006; Delorme-Walker *et al.*, 2011). Pressure exerted on the F-actin network via the opposing membrane tension also contributes a rearward stress on the actin network (Ji *et al.*, 2008). The resulting sum of these stresses, directed away from the leading edge, is distributed in a consistent way between the stress borne by the adhesion-based clutch and the remainder, which results in slippage of the network manifest as retrograde flow (Aratyn-Schaus and Gardel, 2010; Walcott and Sun, 2010; Figure 1b). The second mechanical effect captured by the model is the fragility of the adhesion/F-actin linkages under increasing force (Bell, 1978). Thus, when the stress on the F-actin network is not borne by a sufficient density of adhesive bonds, those bonds will collectively fail. Together, the effects of retrograde flow and rupture of the adhesion-based clutch constitute a myosin-based feedback loop that halts protrusion.

Adhesion-mediated biochemical and mechanical feedbacks control the duration and frequency of simulated protrusion events, predictive of distinct behavior as ECM density is varied

The stochastic model was used to simulate leading-edge protrusion dynamics as seen in a local patch of the lamellipodium, systematically varying the parameter that corresponds to the density of ECM. Various studies have shown that cell migration speed varies biphasically as a function of ECM density (e.g., Palecek *et al.*, 1997). The persistence of leading-edge protrusion likely contributes to that relationship (Cirit *et al.*, 2010). Indeed, stochastic simulations of our protrusion model show a biphasic dependence of motility on ECM density (Figure 2). When the ECM density is less than optimal, simulated protrusion events tend to be sporadic and short lived (Figure 2a). They emerge

stochastically and fail because the density of nascent adhesions formed is not sufficient to sustain the core protrusion feedback loop. Another feature of the low-ECM regime is that activation of myosin II is slight. Accordingly, the stress imposed on the F-actin network and the velocity of its retrograde flow are relatively low.

As the ECM density is increased, maintenance of adhesion-mediated signaling is more robust, whereas accumulation of stress mediated by activated myosin II limits the duration of simulated protrusion events. At a near-optimal ECM density, the trade-off between these two opposing effects is balanced, and more persistent protrusion events are observed (Figure 2b). At intermediate ECM densities somewhat greater than the optimal condition, the duration of protrusions is limited by increased retrograde flow velocity, driven by changing myosin activity (Lin *et al.*, 1996). Once retrograde flow outpaces actin polymerization, membrane protrusion and formation of nascent adhesions cease; accumulation of active myosin is rate controlling in this process, and therefore protrusions are shorter lived as the ECM density is increased above optimal levels (Figure 2, c–e). Under these conditions, nascent adhesion density usually peaks after the maximal protrusion velocity is observed; given that nascent adhesions mediate activation of Rac, this result is consistent with the reported delay between protrusion and Rac1 activity (Machacek *et al.*, 2009). Protrusions are also predicted to be less frequent in this regime, limited by the time required to reset myosin activity to a sufficiently low level. At the highest ECM densities evaluated (Figure 2e), the forces exerted on the F-actin–bound adhesions accumulate after cessation of protrusion and become so great that the bonds collectively fail. Later, we will show how failure of the clutch might actually enhance protrusion frequency by hastening the decay of local myosin activity.

The predicted distributions of protrusion durations are nonnormal, consistent with experimental measurements

As the representative model output shows, protrusion velocity tends to switch rapidly between on and off states, suggesting that the stochastic protrusion dynamics for each simulation condition may be comprehensively characterized by the distributions of times spent in the protrusion-on and protrusion-off states. The distribution of simulated protrusion-on times is shown for each of multiple ECM density conditions (Figure 3a), and the corresponding distributions of protrusion-off times are shown in Supplemental Figure S1. For each ECM density, the distribution of protrusion duration times shows a characteristic shape, with the short-lived, stochastic protrusions occurring most frequently and the persistent protrusions observed least frequently. When we compared the distributions of simulated protrusion durations to the distribution constructed from aggregate experimental measurements of optimally migrating mouse fibroblasts, we found similar characteristic protrusion distribution shapes (Figure 3b; data for individual cells are shown in Supplemental Figure S2 and Supplemental Video S1). Another feature of the protrusion duration distribution, which emerges from the simulated dynamics at higher-than-optimum ECM density, is a distinct peak at the high end of protrusion times (Figure 3a). This is caused by the tendency of the model toward more deterministic behavior (oscillations).

To compare distributions across simulation conditions, in which the ECM density parameter and other model parameters were varied, we report both the arithmetic mean and the 98th percentile of each distribution, the latter serving as a practical measure of the longer durations. Together, the mean and 98th percentile reflect the asymmetric shape of each distribution. As expected, by either metric there is an optimum of protrusion duration as a function of ECM density (Figure 3c). The mean protrusion duration also shows a second peak in the range of higher ECM densities ($E > 10$ μm^{-1}), which reflects the change in skewness of the distribution, as shown in Figure 3a. In this regime, increasing the ECM density reduces the duration of the longest-lived protrusions, whereas the incidence of short-lived protrusions is also reduced. Of interest, the maximum protrusion duration is not accompanied by the shortest wait time between protrusions, which is seen at a somewhat higher value of the ECM density parameter (Figure 3c).

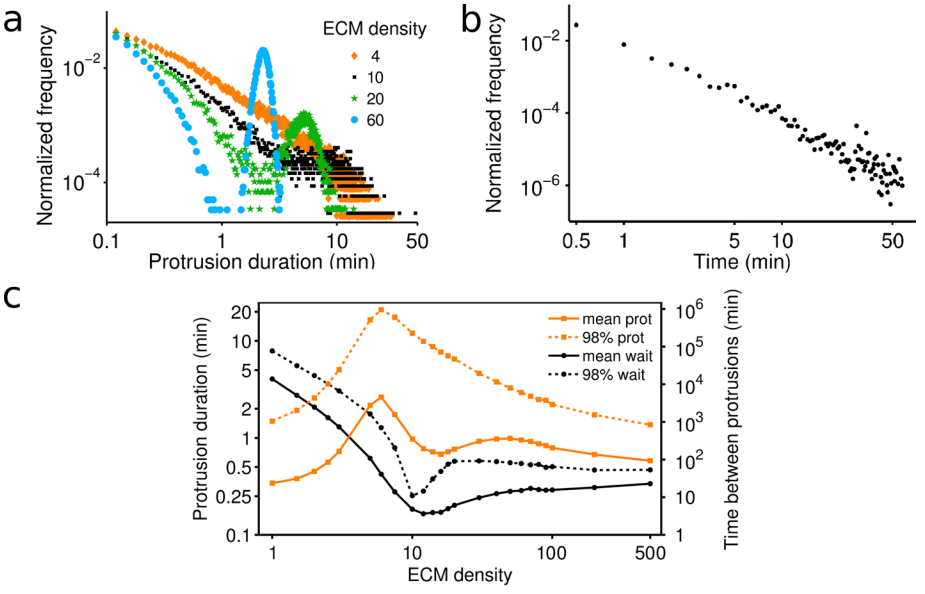

FIGURE 3: Distributions of simulated and measured protrusion duration times. (a) The frequency histogram of protrusion duration times, constructed from model simulation results, shows a broad, nonnormal distribution that shifts as the ECM parameter is modulated. (b) An aggregate frequency histogram of protrusion duration times was constructed from experimental measurements of mouse fibroblasts migrating on fibronectin ($n = 5$). Distributions for the individual cells are shown in Supplemental Figure S2. (c) Ensemble simulation results for the protrusion duration times and the wait times between protrusions. For each value of the ECM density parameter, E (μm^{-1}), each distribution of protrusion-on or -off times is characterized by its arithmetic mean and 98th percentile value.

Model simulations advance the concept that protrusion is optimized by balancing adhesion formation against myosin activation

The sensitivity of the simulated dynamics to the various subprocesses included in the model can be evaluated by modulating the values of the model parameters, which might also reflect the effects of molecular perturbations or comparisons across cell backgrounds. For example, the subset of parameters related to the actin polymerization subcircuit affect the dynamics at low ECM density or shift the entire biphasic curve. Among the more illustrative of those parameters is the actin depolymerization rate constant, k_{DP}. In the model, this parameter affects the steady-state width of the F-actin

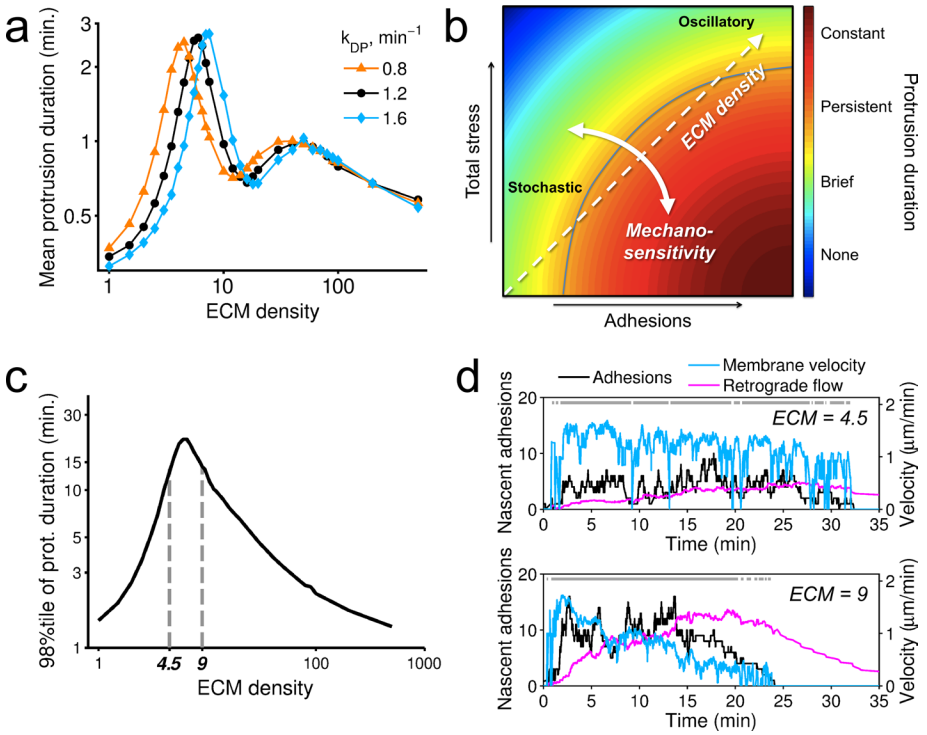

FIGURE 4: Opposing roles of adhesion and contractility in protrusion dynamics. (a) Model parameters that affect F-actin polymerization/depolymerization, such as the depolymerization rate constant, k_{DP}, shift the protrusion duration vs. ECM density curve, except at very high ECM density. (b) Conceptual graph illustrating how optimization of protrusion duration (color bar) reflects a trade-off between generation of adhesions and generation of stress induced primarily by active myosin. The dashed line represents a path of increasing ECM density, which is altered by the mechanosensitivity of myosin activation. (c) The two indicated values of the ECM density parameter, E (μm^{-1}), yield approximately equal protrusion durations. (d) Simulations illustrate the dynamics of total nascent adhesion density and the velocities of actin polymerization and F-actin retrograde flow for the two values of the ECM density parameter highlighted in c. The gray bars at the top of each plot mark intervals in the protrusion-on state.

network and sets the time scale for its dynamic response to a change in polymerization rate. In turn, the lamellipodial width affects adhesion turnover, since nascent adhesions disintegrate once the F-actin network has moved completely over them (Vicente-Manzanares *et al.*, 2009a). As expected, simulations show that increasing (decreasing) actin depolymerization frequency shifts the protrusion duration curve toward higher (lower) ECM density, by decreasing (increasing) the numbers of F-actin–bound adhesions (Figure 4a). At the highest ECM densities, however, the protrusion dynamics are insensitive to actin depolymerization (Figure 4a). Under these conditions, the rise in retrograde flow is faster than adhesion turnover, and therefore protrusions do not persist long enough for the nascent adhesion density to reach a plateau level.

The simulations suggest a conceptual model in which the balance between adhesion formation and generation of stress through myosin II determines protrusion persistence. As illustrated in Figure 4b, both nascent adhesion abundance and activation of myosin increase with ECM density, and their opposing effects define an optimal condition for protrusion. To exemplify this view of the model, we examined simulations for values of the ECM density parameter on either side of the optimum (Figure 4c). As expected, the same near-optimal protrusion condition can be achieved with lower (higher) abundance of nascent adhesions combined with lower (higher) stress exerted by myosin on the F-actin network; as a consequence, retrograde flow catches up with actin polymerization to halt the longest-lived protrusions after roughly the same duration for the lower and higher ECM values (98th percentile values of 13.3 and 14.1 min, respectively). Excerpts from the simulations clearly show that the distributions of protrusion durations are not the same, however; the lower ECM value yields a higher incidence of protrusions of intermediate duration (Figure 4d; see also Figure 3a) and thus a higher mean (1.74 min, as compared with 1.25 min for the higher ECM). As we explore, the balance between adhesion formation and stress generation is altered by varying model parameters that affect the mechanosensitivity of myosin activation (Figure 4b).

Modulating myosin abundance is predicted to dramatically alter protrusion dynamics at higher, but not at lower, ECM densities

The foregoing analysis suggests that optimal conditions for protrusion satisfy a compromise between two adhesion-based feedback loops, with mechanical tension on F-actin–bound adhesions and activation of myosin constituting the basis for the feedback loop that reins in protrusion. The mechanosensitivity of this circuit can be modulated experimentally by affecting myosin abundance/activity or possibly by varying the stiffness of the adhesive substratum material. In our simulation framework, decreasing myosin abundance (as if by RNA interference or, analogously, by treatment with blebbistatin) allows for a higher optimum in protrusion duration, achieved at a modestly higher ECM density, and generally increases the durations of the longer-lived protrusions at intermediate and high ECM densities (Figure 5a). This result stands in qualitative agreement with experimental observations that loss of function of myosin II (Vicente-Manzanares *et al.*, 2007; Cirit *et al.*, 2010; Lim *et al.*, 2010; Burnette *et al.*, 2011) or of RhoA signaling (Totsukawa *et al.*, 2004) enhances protrusion. Further, because of the nonlinear nature of the feedback loop, the simulations predict an ultrasensitive dependence of optimal protrusion duration on myosin abundance. Our simulations also suggest that modulation of myosin abundance or activity has little effect on protrusion when ECM density is less than the optimum, which might explain why certain measurements show no discernible effect of myosin inhibition on protrusion (Giannone *et al.*, 2007).

Another potential readout of lamellipodial mechanics is the velocity of retrograde flow. Simulations show that, for intermediate ECM densities, increasing myosin abundance results in increased retrograde flow (averaged during periods of protrusion), but the relationship is saturable; at higher myosin abundance, average retrograde flow velocity plateaus (Figure 5b). The simulations show why this is the case: higher myosin abundance hastens the increase in retrograde flow, but during the (shorter) cycle of protrusion, the velocity of retrograde flow spans roughly the same range of values (Figure 5c). In general, the simulation results agree with experimental observations detailing the temporal characteristics of actin and myosin in the lamellipodium during a protrusion event (Burnette

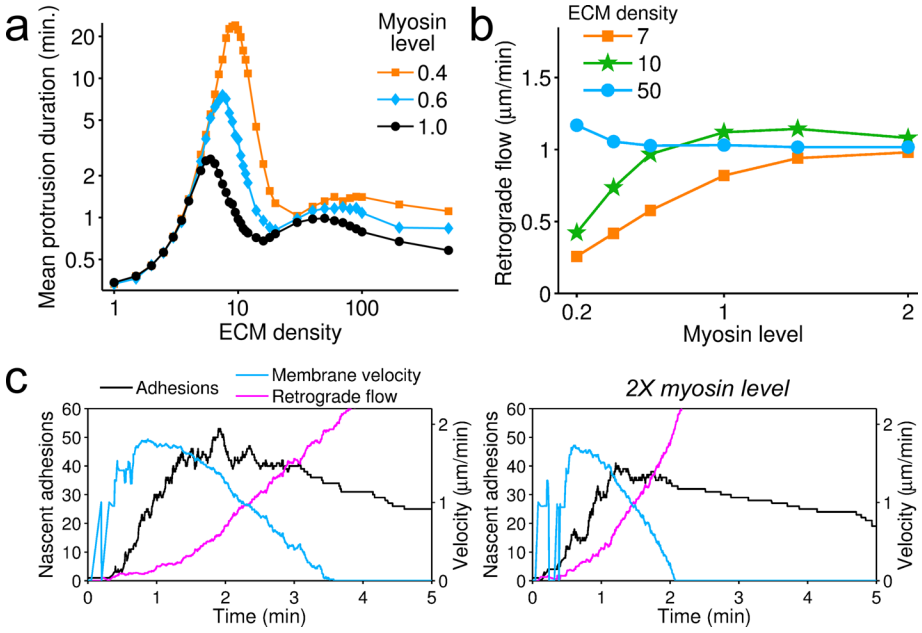

FIGURE 5: Sensitivity of the simulated protrusion dynamics to myosin abundance. (a) Myosin knockdown or inhibition was simulated by modulating the activation parameter, $k_{a,m}$; myosin level refers to the value of this parameter relative to the base case. Reducing myosin contractility results in an ultrasensitive increase in the mean duration of protrusion, except when the ECM density parameter, E (μm^{-1}), is low. (b) Simulated retrograde flow velocities, time-averaged during the protrusion-on periods, exhibit a saturable dependence on myosin abundance but are strongly sensitive to ECM density in the model. (c) Representative simulation results for $E = 40$ μm^{-1} compare the base case to a scenario with myosin abundance doubled.

et al., 2011): myosin was found to be lacking during the initial phase of protrusion, followed by myosin accumulation and a sharp increase in retrograde flow before protrusion stops (Figure 5c).

The effect of varying ECM density on the average retrograde flow parallels the effect of varying myosin abundance. When myosin abundance is low, average retrograde flow is an increasing function of ECM density, in qualitative agreement with experimental measurements that showed an increase in retrograde flow in the lamellipodium with increasing ECM (Gupton and Waterman-Storer, 2006); in the high-myosin regime, average retrograde flow velocity saturates (Figure 5b). The effects of varying ECM density differ depending on whether retrograde flow is measured in the lamellipodium or in the lamellum (Gardel *et al.*, 2008), and our simulations suggest that the timing relative to the onset and cessation of protrusion will also affect measured retrograde flow values. Therefore, when comparing such predictions to experimental observations, it will be important to distinguish both the spatial location (lamellipodium vs. lamellum) and timing (relative to protrusion) of the retrograde flow measurements.

Retrograde flow and fragility of the adhesion-based clutch are predicted to affect protrusion failure in distinct ways

Having assessed the influence of myosin-dependent stress on the F-actin network, we sought to modulate the mechanisms by which the stress is dissipated: through resistances associated with retrograde flow and the adhesion-based clutch. In the model, the distribution of stress between the two depends on the abundance of F-actin-bound adhesions; the more bonds there are, the more they collectively resist the stress. The velocity of retrograde flow that results from the remaining stress, relative to the velocity of F-actin polymerization, determines the attendant protrusion dynamics. As outlined in the *Discussion*, this sort of mechanical model might offer useful insight (at least conceptually) into how leading-edge motility is perturbed in cells migrating on mechanically soft substrates.

As one might expect, reducing the resistance to retrograde flow, characterized by the parameter ξ, affects the duration of protrusion in essentially the same manner as an increase in the yield of myosin activation (Figure 6, a and b; compare Figure 6b to Figure 5c). Both increase the acceleration (but not the average velocity) of retrograde flow during protrusion, and thus the protrusion event is shorter in duration.

Far less intuitive is the effect of modulating clutch fragility, which is characterized by the F-actin-adhesion bond compliance, f_c. This parameter is formulated in units of force borne by each nascent adhesion in complex with the F-actin network, a bond composed of multiple interactions. When the force distributed among these interactions exceeds the value of f_c, the bond tends to dissociate. As explained in the Supplemental Materials and Methods, the model predicts a direct relationship between the force per bond and the retrograde flow velocity. Protrusion stops when retrograde flow outpaces actin polymerization, defining a critical force f_{crit} above which protrusion cannot occur (Figure 6c). For the base-case parameters, the bond compliance is far greater than this critical force, allowing F-actin–bound adhesions to activate myosin after protrusion ceases. For a reduced f_c value, set equal to f_{crit}, the duration of protrusion is essentially unchanged; the retrograde flow velocity needed to halt protrusion is associated with the same build-up of force. The difference is that cessation of protrusion is concomitant with clutch failure, interrupting the activation of myosin and allowing the system to reset sooner (Figure 6c). When the value of f_c is reduced further, well below that of f_{crit}, the clutch is forced to oscillate between load and fail states, whereas myosin activity hovers around a characteristic value (Figure 6c). As explained in the Supplemental Materials and Methods, this level of myosin activity is associated with the minimum stress needed to elicit retrograde flow that outpaces maximal actin polymerization.

DISCUSSION

The present physicochemical model of leading-edge dynamics integrates aspects of integrin-mediated signaling and cytoskeletal mechanics, formulated at a level of granularity that allows a systematic analysis of their interplay. The signaling module is a stripped-down version of the core positive feedback loop described previously (Cirit *et al.*, 2010; Welf and Haugh, 2010); when coupled with negative regulation, the previous models and the present one successfully capture the biphasic dependence of protrusion dynamics on ECM density and the stochastic nature of protrusion at low ECM density. The inclusion of mechanics in the present model offers a new, physically based description of the negative regulatory loop that limits protrusion duration at high ECM density. The interpretation is that protrusion ceases as a consequence of mechanosensitive activation of myosin II, which mediates increased retrograde flow and, under certain conditions, failure of the adhesion-based clutch.

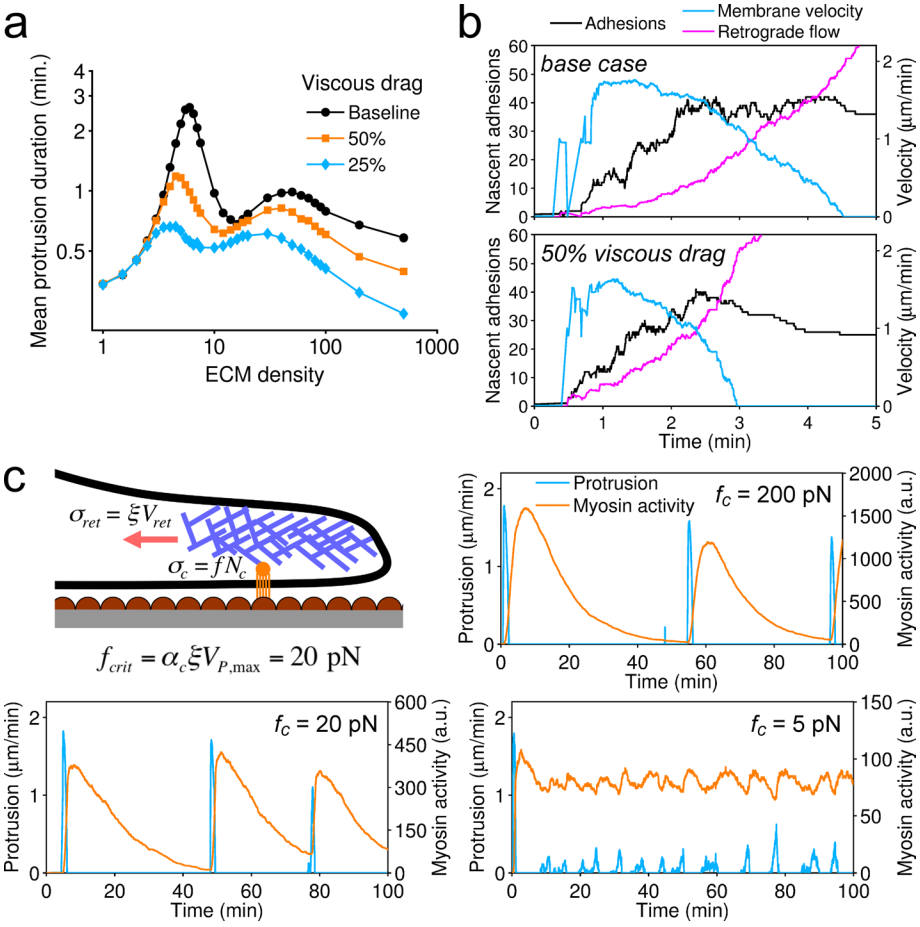

FIGURE 6: Retrograde flow and clutch bond fragility affect the protrusion circuit in distinct ways. (a) A modest reduction in viscous drag resisting retrograde flow compromises protrusion, except when ECM density is low. (b) Simulation results, with $E = 40$ μm^{-1}, suggest that protrusion duration is reduced because retrograde flow overwhelms actin polymerization more abruptly, in the same manner as an increase in myosin abundance. (c) The diagram illustrates the distribution of stress dissipated by retrograde flow (σ_{ret}) and the adhesion-based clutch (σ_c). When the force per bond, f, exceeds a critical value f_{crit}, leading-edge protrusion cannot occur. Simulation results, with $E = 200$ μm^{-1}, predict that a more fragile clutch (lower value of f_c) can generate more frequent protrusions.

In the process, the model makes contact with existing biophysical measurements, including lamellipodial width, actin polymerization velocity, retrograde flow velocity, and traction stress. The model was used to simulate manipulations of myosin expression in combination with variation of ECM density, and the trends we report are qualitatively consistent with published experiments. As we now outline in more detail, analysis of the model also suggests new concepts that may be evaluated through quantitative experiments designed to test the hypotheses inherent in the model's construction.

Unlike deterministic models, stochastic models generate simulated data sets with fluctuations that can be compared with those seen in live-cell data. Perhaps the most intriguing emergent property of the present model is the broad distribution of protrusion durations, which shows a characteristic shape. This key feature of the model was validated through analysis of live-cell migration videos. Certainly, the protrusion times extracted from both simulations and experiments are not normally distributed, suggesting that the typical statistical comparisons might not be appropriate and that the shape of the distribution should be carefully considered when characterizing protrusion dynamics from experiments. We propose that the dynamics of individual protrusion events and the aggregate distributions thereof provide valuable information about local protrusion that is lost by studying population averages. For example, a comparison of mean protrusion durations showed no significant effect of the myosin inhibitor, blebbistatin (Giannone *et al.*, 2007). In the context of our model, this result is expected if the ECM density is even modestly below the optimum. Yet even under such conditions it might be possible to discern a subtle change in the distribution of protrusion durations.

At higher-than-optimum ECM density, the simulated distributions also show a distinct peak at the high end of protrusion times (Figure 3a), a sign of more deterministic behavior. In reality, such regular oscillations would be less likely to appear because of additional sources of noise not considered in the present model, such as the subcellular distributions of myosin II (Gupton and Waterman-Storer, 2006; Vicente-Manzanares *et al.*, 2007) and G-actin (Katz *et al.*, 2012). Nevertheless, in certain experimental contexts regular oscillations of leading-edge protrusion have been reported, and this phenomenon has been explained using mathematical modeling (Wolgemuth, 2005; Chan and Odde, 2008; Enculescu *et al.*, 2010; Ryan *et al.*, 2012). These models and ours differ with respect to the subprocesses that are emphasized and the precise nature of the negative feedback that reins in protrusion. In Wolgemuth's model, stress is driven by a gradient in F-actin density, although he also considered the possibility of myosin motor–induced stress, which was postulated to increase according to the F-actin density (Wolgemuth, 2005). In their model of growth cone filopodia, Chan and Odde (2008) considered myosin-induced stress, and like Wolgemuth they reasoned that the protrusion fails when adhesive bonds rupture. The model of Enculescu *et al.* (2010) does not explicitly describe adhesion to the substratum, focusing instead on attachment/detachment of actin filaments at the membrane boundary that naturally fluctuates in tandem with mechanical compression/relaxation of the F-actin network. Finally, Ryan *et al.* (2012) proposed that the increase in F-actin density during protrusion feeds back to inhibit the generation of new barbed ends; that is, control is entirely at the level of F-actin polymerization. This view is consistent with experiments showing that retrograde flow is invariant in their system. By comparison, our model focuses on adhesion dynamics and activation of myosin through adhesion-mediated feedback. Under conditions in which our model produces oscillations, the hallmarks of protrusion deceleration and cessation are accumulation of myosin activity and increased retrograde flow, in line with reported observations (Burnette *et al.*, 2011).

Other concepts emerging from this analysis concern the dynamic mechanisms that mechanically regulate the lamellipodium. In the model, stress on the F-actin network is distributed between an

adhesion-based clutch and retrograde flow, and rearrangement of the underlying equations revealed a linear relationship between the force exerted on each F-actin–bound nascent adhesion and the retrograde flow velocity. Although this prediction relies on simplifying assumptions, it presents a plausible and testable hypothesis. The other aspect of lamellipodial mechanics is the fragility of F-actin–adhesion bonds. Our simulations suggest that this parameter could be precisely tuned so that cessation of protrusion, brought about by increased retrograde flow, is accompanied by failure of the clutch. With fewer adhesions under tension, local myosin activity relaxes faster, allowing the system to reset more efficiently. If this were the case in migrating cells, it would be possible to diagnose by tracking the slip of F-actin relative to nascent adhesions.

Although it is widely speculated that adhesion and lamellipodial F-actin mechanics largely determine cell spreading and motility responses on soft materials, the mechanisms by which cells sense and respond to substratum stiffness are not well understood (Bershadsky *et al.*, 2006). The general observations are that cell spreading and traction stress monotonically increase as a function of stiffness, whereas cell migration speed is optimized at an intermediate stiffness value that is reduced as the ECM density is increased (Peyton and Putnam, 2005; Stroka and Aranda-Espinoza, 2009; Shebanova and Hammer, 2012). The concept that substratum stiffness enhances the efficiency of adhesion formation for a given ECM density seems to unify these observations and has solid theoretical support (Paszek *et al.*, 2009); however, cell speed is a macroscopic readout that integrates multiple, subcellular processes. In light of our analysis, an analogous data set quantifying protrusion duration and frequency statistics, preferably in conjunction with live-cell imaging of adhesion or F-actin dynamics, might be more mechanistically insightful. In the context of our model, the proposed mechanism of adhesion clustering efficiency increasing with stiffness could be incorporated at a coarse-grained level as a shift in the ECM density parameter, but other possible mechanisms may also be considered. One is that migration on a soft surface might alter the distribution of stress, manifest as the slope/shape of the aforementioned force–retrograde flow relationship. A simple yet new idea along that line, consistent with recent experimental measurements (Aratyn-Schaus and Gardel, 2010), is that substratum compliance reduces the resistance to retrograde flow. The physical interpretation is that forward movement is reduced by the rearward deflection of the surface, thus limiting protrusion duration on soft surfaces. A different but not mutually exclusive mechanism is that substratum compliance might dissipate a fraction of the tension exerted on F-actin–bound adhesions. In the present model, this effect is cast as a more robust (less fragile) clutch mechanism and reduced mechanosensitive feedback to myosin II, which would offset at least partially the aforementioned reduction in protrusion duration. As outlined here, multiplexed measurements of protrusion statistics, retrograde flow, and traction stress will be needed to deconvolute these interwoven effects.

Cell migration speed is a complex function of protrusion and retraction dynamics (Burnette *et al.*, 2011). The present model of leading-edge protrusion is minimally detailed and intended as a starting point for incorporating greater mechanistic detail and integrating multiple subprocesses that together determine overall cell migration speed and persistence. In terms of biological mechanisms, one could add details about the signaling pathways mediated by integrins and by other cell surface receptors that sense spatial cues, as in chemotaxis, for example, along with details of how those pathways modify F-actin (Ditlev *et al.*, 2009). In terms of the model's physics, the primary refinement that would need to be addressed is to move toward a spatially extended stochastic framework, which would allow for proper accounting of variation in F-actin density and nucleotide state as a function of position (relative to the membrane boundary and along its contour), for example. As demonstrated in other models of cell motility, spatial models can incorporate and couple diffusion and advection of molecular components (Mogilner and Edelstein-Keshet, 2002; Ditlev *et al.*, 2009; Cirit *et al.*, 2010), F-actin rheology (Rubinstein *et al.*, 2005, 2009; Shemesh *et al.*, 2012), and the self-organization of myosin (Barnhart *et al.*, 2011; Stachowiak *et al.*, 2012). Thus the prospect of integrating the different F-actin and adhesion mechanics in the lamellipodial and lamellar regions (Gardel *et al.*, 2008) should be approachable. Of course, model refinements generally increase the burden of adding new adjustable parameters and modeling assumptions, and hence it will be important to build such models in concert with quantitative live-cell imaging and other experimental advances.

MATERIALS AND METHODS

Modeling

For compactness, the model is presented here as a system of ordinary differential equations and associated algebraic relations. The conversion of this deterministic system into a stochastic model and the implementation of stochastic simulations were performed as previously described (Welf and Haugh, 2012). Stochastic variables are updated in time using a Gillespie-based formalism (Gillespie, 1977), implemented in MATLAB (MathWorks, Natick, MA) using the next-reaction method (Gibson and Bruck, 2000). Thus noise arises from fluctuations in the numbers of each species in the control volume. All pertinent details of the simulations and a fuller discussion of the underlying model assumptions and parameter estimates are provided in the Supplemental Materials and Methods.

The width of the lamellipodium, δ (μm), changes according to the rates of F-actin polymerization and depolymerization. The polymerization velocity, V_P, is a saturable function of active Rac, density R (Cirit *et al.*, 2010; Welf and Haugh, 2010). The depolymerization velocity is proportional to δ, with rate constant k_{DP}, consistent with theory (Michalski and Carlsson, 2010):

$$\frac{d\delta}{dt} = V_P(R) - k_{DP}\delta$$
$$V_P(r) = \left(V_{P,0} + V_{P,\max}K_v R\right)/\left(1 + K_v R\right) \quad (1)$$

Activation of Rac signaling is mediated by nascent adhesions, density N. The rates of adhesion formation and turnover depend on the velocity of membrane protrusion, V_{mem} (Chang and Hammer, 1999; Choi *et al.*, 2008), which determines the throughput of immobile adhesions as the F-actin network moves forward. The adjusted parameter E (μm^{-1}) defines the efficiency of nascent adhesion formation and is a (not necessarily linear) function of the ECM density (Cirit *et al.*, 2010; Welf and Haugh, 2010):

$$\frac{dN}{dt} = V_{\text{mem}}E - \left(k_{d,n} + \frac{V_{\text{mem}}}{\delta}\right)N$$
$$\frac{dR}{dt} = k_{a,r}N - k_{d,r}R \quad (2)$$

Base parameter values for this part of the model were fixed at $V_{P,\max} = 2$ μm/min (Pollard *et al.*, 2000), $V_{P,0} = 0.005$ μm/min, $K_V = 1$, $k_{DP} = 1.2$ min^{-1} (Rubinstein *et al.*, 2009), $k_{d,n} = 0.2$ min^{-1}, $k_{a,r} = 4$ min^{-1}, and $k_{d,r} = 4$ min^{-1} (Moissoglu *et al.*, 2006).

Equations 1 and 2 constitute a protrusion-based positive feedback loop (Cirit *et al.*, 2010; Welf and Haugh, 2010). In the present

model, we account more explicitly for the mechanics that determines the F-actin retrograde flow velocity, V_{ret}, which offsets actin polymerization according to $V_{mem} = V_P - V_{ret}$ (Barnhart *et al.*, 2011). We impose a mechanical stress balance, by which the imposed rearward stress σ, with contributions from boundary pressure and the action of myosin (σ_b and σ_{myo}, respectively), is opposed by the collective tension on the adhesion-based clutch, σ_c, and by dissipation associated with retrograde flow, stress σ_{ret}. These quantities are expressed as forces (in pN) distributed over the projected area of the F-actin network in the simulated compartment. For simplicity we assume linear relationships relating σ_b to V_{mem} and σ_{ret} to V_{ret} (Barnhart *et al.*, 2011), and we define the density of active myosin M:

$$\begin{aligned}\sigma &= \sigma_b + \sigma_{myo} = \sigma_c + \sigma_{ret}\\ \alpha_b V_{mem} + \alpha_{myo} M &= \sigma_c + \xi V_{ret}\end{aligned} \tag{3}$$

As explained in more detail in the Supplemental Materials and Methods, we reason that the distribution of stress between σ_c and σ_{ret} depends on the F-actin–bound adhesion density N_c. Another, mathematically equivalent way of casting this argument is that V_{ret} is related to total stress σ by a friction coefficient that is an increasing function of N_c (Barnhart *et al.*, 2011):

$$\frac{\sigma_c}{\sigma} = \frac{\alpha_c N_c}{1 + \alpha_c N_c} \tag{4}$$

Base parameter values here were fixed at α_b = 10 pN-min/μm, α_{myo} = 5 pN, ξ = 200 pN-min/μm, and α_c = 0.05. Parameterization here was based on estimates of forces imposed on adhesions and retrograde flow velocities reported in the literature (Munevar *et al.*, 2001; Gardel *et al.*, 2008; Grashoff *et al.*, 2010), as discussed in the Supplemental Materials and Methods.

We assume that the aforementioned clutch is composed of nascent adhesion complexes (density N_c) that are bound to the F-actin network (Chan and Odde, 2008). We assume that the densities of bound and unbound adhesions are close to equilibrium and that the equilibrium is perturbed by the applied force f borne by each bond (which is composed of multiple molecular interactions); we apply the Boltzmann-like relationship attributed to Bell (1978) to model the rupture of adhesive bonds under force:

$$\begin{aligned}\frac{N_c}{N} &= \frac{K_c(f)}{1 + K_c(f)}\\ K_c(f) &= K_{c,0}\exp(-f/f_c)\\ f &= \sigma_c / N_c\end{aligned} \tag{5}$$

Tension on the clutch adhesions also feeds back to enhance myosin activation, in accord with a mechanosensitive, Rho-dependent pathway (Guilluy *et al.*, 2011). The Boltzmann representation is used here again to distinguish those F-actin–bound adhesions that are capable of mediating myosin activation (density N_{c^*}); this equilibrium responds positively to force:

$$\begin{aligned}\frac{dM}{dt} &= k_{a,m} N_{c^*} - k_{d,m} M\\ N_{c^*} / N_c &= K_{c^*}(f) / [1 + K_{c^*}(f)]\\ K_{c^*}(f) &= K_{c^*,0}\exp(f / f_{c^*})\end{aligned} \tag{6}$$

Base parameter values for this part of the model were fixed at $K_{c,0}$ = 1.5 and f_c = 200 pN, $k_{a,m}$ = 0.5 min^{-1}, $k_{d,m}$ = 0.1 min^{-1}, $K_{c^*,0}$ = 1, and f_{c^*} = 10 pN. These values were assigned as described in the Supplemental Materials and Methods.

Experimental

Experiments using NIH 3T3 cells (American Type Culture Collection, Rockville, MD), expressing a green fluorescent protein (GFP)–tagged protein (GFP-AktPH) and randomly migrating on fibronectin-coated cover slips, were conducted as described previously (Welf *et al.*, 2012). The contact area of each cell was imaged by total internal reflection fluorescence microscopy and segmented as described previously (Welf *et al.*, 2012). A 63×, 1.0 numerical aperture water immersion objective (Carl Zeiss, Thornwood, NY) was used, and the time interval between frames was 5 s. Protruded pixels were grouped according to their proximity in space and continuity in time (Supplemental Materials and Methods and Supplemental Figure S3).

ACKNOWLEDGMENTS

We thank James Bear (University of North Carolina, Chapel Hill, NC), Gaudenz Danuser (Harvard Medical School, Boston, MA), and Alex Mogilner (University of California, Davis, CA) for helpful discussions. This work was supported by National Science Foundation Grant CBET-1133476, and E.S.W. was supported by the Cell Migration Consortium under National Institutes of Health Grant U54-GM064346.

REFERENCES

Alexandrova AY, Arnold K, Schaub S, Vasiliev JM, Meister JJ, Bershadsky AD, Verkhovsky AB (2008). Comparative dynamics of retrograde actin flow and focal adhesions: formation of nascent adhesions triggers transition from fast to slow flow. PLoS One 3, e3234.

Aratyn-Schaus Y, Gardel ML (2010). Transient frictional slip between integrin and the ECM in focal adhesions under myosin II tension. Curr Biol 20, 1145–1153.

Barnhart EL, Lee KC, Keren K, Mogilner A, Theriot JA (2011). An adhesion-dependent switch between mechanisms that determine motile cell shape. PLoS Biol 9, e1001059.

Bell GI (1978). Models for the specific adhesion of cells to cells. Science 200, 618–627.

Bershadsky A, Kozlov M, Geiger B (2006). Adhesion-mediated mechanosensitivity: a time to experiment, and a time to theorize. Curr Opin Cell Biol 18, 743–781.

Boettiger D (2012). Mechanical control of integrin-mediated adhesion and signaling. Curr Opin Cell Biol 24, 592–599.

Brown CM, Hebert B, Kolin DL, Zareno J, Whitmore L, Horwitz AR, Wiseman PW (2006). Probing the integrin-actin linkage using high-resolution protein velocity mapping. J Cell Sci 119, 5204–5214.

Brown ME, Bridgman PC (2003). Retrograde flow rate is increased in growth cones from myosin IIB knockout mice. J Cell Sci 116, 1087–1094.

Burnette DT, Manley S, Sengupta P, Sougrat R, Davidson MW, Kachar B, Lippincott-Schwartz J (2011). A role for actin arcs in the leading-edge advance of migrating cells. Nat Cell Biol 13, 371–381.

Cai YF *et al.* (2006). Nonmuscle myosin IIA-dependent force inhibits cell spreading and drives F-actin flow. Biophys J 91, 3907–3920.

Carlsson AE, Sept D (2008). Mathematical modeling of cell migration. Methods Cell Biol 84, 911–937.

Chan CE, Odde DJ (2008). Traction dynamics of filopodia on compliant substrates. Science 322, 1687–1691.

Chang KC, Hammer DA (1999). The forward rate of binding of surface-tethered reactants: effect of relative motion between two surfaces. Biophys J 76, 1280–1929.

Choi CK, Vicente-Manzanares M, Zareno J, Whitmore LA, Mogilner A, Horwitz AR (2008). Actin and α-actinin orchestrate the assembly and maturation of nascent adhesions in a myosin II motor-independent manner. Nat Cell Biol 10, 1039–1050.

Cirit M, Krajcovic M, Choi CK, Welf ES, Horwitz AF, Haugh JM (2010). Stochastic model of integrin-mediated signaling and adhesion dynamics at the leading edges of migrating cells. PLoS Comput Biol 6, e1000688.

Cox EA, Sastry SK, Huttenlocher A (2001). Integrin-mediated adhesion regulates cell polarity and membrane protrusion through the Rho family of GTPases. Mol Biol Cell 12, 265–277.
Danuser G (2011). Computer vision in cell biology. Cell 147, 973–978.
Delorme-Walker VD, Peterson JR, Chernoff J, Waterman CM, Danuser G, DerMardirossian C, Bokoch GM (2011). Pak1 regulates focal adhesion strength, myosin IIA distribution, and actin dynamics to optimize cell migration. J Cell Biol 193, 1289–1303.
DiMilla PA, Barbee K, Lauffenburger DA (1991). Mathematical model for the effects of adhesion and mechanics on cell migration speed. Biophys J 60, 15–37.
Ditlev JA, Vacanti NM, Novak IL, Loew LM (2009). An open model of actin dendritic nucleation. Biophys J 96, 3529–3542.
Enculescu M, Sabouri-Ghomi M, Danuser G, Falcke M (2010). Modeling of protrusion phenotypes driven by the actin-membrane interaction. Biophys J 98, 1571–1581.
Gardel ML, Sabass B, Ji L, Danuser G, Schwarz US, Waterman CM (2008). Traction stress in focal adhesions correlates biphasically with actin retrograde flow speed. J. Cell Biol 183, 999–1005.
Gardel ML, Schneider IC, Aratyn-Schaus Y, Waterman CM (2010). Mechanical integration of actin and adhesion dynamics in cell migration. Annu Rev Cell Dev Biol 26, 315–333.
Giannone G *et al.* (2007). Lamellipodial actin mechanically links myosin activity with adhesion-site formation. Cell 128, 561–575.
Gibson MA, Bruck J (2000). Efficient exact stochastic simulation of chemical systems with many species and many channels. J Phys Chem A 104, 1876–1889.
Gillespie DT (1977). Exact stochastic simulation of coupled chemical reactions. J Phys Chem 81, 2340–2361.
Grashoff C *et al.* (2010). Measuring mechanical tension across vinculin reveals regulation of focal adhesion dynamics. Nature 466, 263–266.
Guilluy C, Swaminathan V, Garcia-Mata R, O'Brien ET, Superfine R, Burridge K (2011). The Rho GEFs LARG and GEF-H1 regulate the mechanical response to force on integrins. Nat Cell Biol 13, 722–727.
Gupton SL, Waterman-Storer CM (2006). Spatiotemporal feedback between actomyosin and focal-adhesion systems optimizes rapid cell migration. Cell 125, 1361–1374.
Henson JH, Svitkina TM, Burns AR, Hughes HE, MacPartland KJ, Nazarian R, Borisy GG (1999). Two components of actin-based retrograde flow in sea urchin coelomocytes. Mol Biol Cell 10, 4075–4090.
Hu K, Ji L, Applegate KT, Danuser G, Waterman-Storer CM (2007). Differential transmission of actin motion within focal adhesions. Science 315, 111–115.
Hu LH, Papoian GA (2011). How does the antagonism between capping and anti-capping proteins affect actin network dynamics. J Phys Condens Matter 23, 374101.
Hughes-Alford SK, Lauffenburger DA (2012). Quantitative analysis of gradient sensing: towards building predictive models of chemotaxis in cancer. Curr Opin Cell Biol 24, 284–291.
Huttenlocher A, Horwitz AR (2011). Integrins in cell migration. Cold Spring Harb Perspect Biol 3, a005074.
Ji L, Lim J, Danuser G (2008). Fluctuations of intracellular forces during cell protrusion. Nat Cell Biol 10, 1393–1400.
Jurado C, Haserick JR, Lee J (2005). Slipping or gripping? Fluorescent speckle microscopy in fish keratocytes reveals two different mechanisms for generating a retrograde flow of actin. Mol Biol Cell 16, 507–518.
Katz ZB, Wells AL, Park HY, Wu B, Shenoy SM, Singer RH (2012). β-Actin mRNA compartmentalization enhances focal adhesion stability and directs cell migration. Genes Dev 26, 1885–1890.
Kuo JC, Han XM, Hsiao CT, Yates JR, Waterman CM (2011). Analysis of the myosin-II-responsive focal adhesion proteome reveals a role for beta-Pix in negative regulation of focal adhesion maturation. Nat Cell Biol 13, 383–393.
Lauffenburger DA, Horwitz AF (1996). Cell migration: a physically integrated molecular process. Cell 84, 359–369.
Lee HS, Anekal P, Lim CJ, Liu CC, Ginsberg MH (2013). Two modes of integrin activation form a binary molecular switch in adhesion maturation. Mol Biol Cell 24, 1354–1362.
Lim JI, Sabouri-Ghomi M, Machacek M, Waterman CM, Danuser G (2010). Protrusion and actin assembly are coupled to the organization of lamellar contractile structures. Exp Cell Res 316, 2027–2041.
Lin CH, Espreafico EM, Mooseker MS, Forscher P (1996). Myosin drives retrograde F-actin flow in neuronal growth cones. Neuron 16, 769–782.
Macdonald A, Horwitz AR, Lauffenburger DA (2008). Kinetic model for lamellipodal actin-integrin "clutch" dynamics. Cell Adh Migr 2, 25–35.
Machacek M, Danuser G (2006). Morphodynamic profiling of protrusion phenotypes. Biophys J 90, 1439–1452.
Machacek M, Hodgson L, Welch C, Elliott H, Pertz O, Nalbant P, Abell A, Johnson GL, Hahn KM, Danuser G (2009). Coordination of Rho GTPase activities during cell protrusion. Nature 461, 99–103.
Maree AFM, Grieneisen VA, Edelstein-Keshet L (2012). How cells integrate complex stimuli: the effect of feedback from phosphoinositides and cell shape on cell polarization and motility. PLOS Comput Biol 8, e1002402.
Michalski PJ, Carlsson AE (2010). The effects of filament aging and annealing on a model lammellipodium undergoing disassembly by severing. Phys Biol 7, 026004.
Mogilner A (2009). Mathematics of cell motility: have we got its number? J Math Biol 58, 105–134.
Mogilner A, Edelstein-Keshet L (2002). Regulation of actin dynamics in rapidly moving cells: a quantitative analysis. Biophys J 83, 1237–1258.
Moissoglu K, Slepchenko BM, Meller N, Horwitz AF, Schwartz MA (2006). In vivo dynamics of Rac-membrane interactions. Mol Biol Cell 17, 2770–2779.
Munevar S, Wang YL, Dembo M (2001). Traction force microscopy of migrating normal and H-ras transformed 3T3 fibroblasts. Biophys J 80, 1744–1757.
Nayal A, Webb DJ, Brown CM, Schaefer EM, Vicente-Manzanares M, Horwitz AR (2006). Paxillin phosphorylation at Ser273 localizes a GIT1-PIX-PAK complex and regulates adhesion and protrusion dynamics. J Cell Biol 173, 587–599.
Palecek SP, Loftus JC, Ginsberg MH, Lauffenburger DA, Horwitz AF (1997). Integrin-ligand binding properties govern cell migration speed through cell-substratum adhesiveness. Nature 385, 537–540.
Parsons JT, Horwitz AR, Schwartz MA (2010). Cell adhesion: integrating cytoskeletal dynamics and cellular tension. Nat Rev Mol Cell Biol 11, 633–643.
Paszek MJ, Boettiger D, Weaver VM, Hammer DA (2009). Integrin clustering is driven by mechanical resistance from the glycocalyx and the substrate. PLoS Comput Biol 5, e1000694.
Peyton SR, Putnam AJ (2005). Extracellular matrix rigidity governs smooth muscle cell motility in a biphasic fashion. J Cell Physiol 204, 198–209.
Pollard TD, Blanchoin L, Mullins RD (2000). Molecular mechanisms controlling actin filament dynamics in nonmuscle cells. Annu Rev Biophys Biomol Struct 29, 545–576.
Ponti A, Machacek M, Gupton SL, Waterman-Storer CM, Danuser G (2004). Two distinct actin networks drive the protrusion of migrating cells. Science 305, 1782–1786.
Ridley AJ, Schwartz MA, Burridge K, Firtel RA, Ginsberg MH, Borisy G, Parsons TJ, Horwitz AR (2003). Cell migration: integrating signals from front to back. Science 302, 1704–1709.
Riveline D, Zamir E, Balaban NQ, Schwarz US, Ishizaki T, Narumiya S, Kam Z, Geiger B, Bershadsky AD (2001). Focal contacts as mechanosensors: externally applied local mechanical force induces growth of focal contacts by an mDia1-dependent and ROCK-independent mechanism. J Cell Biol 153, 1175–1185.
Rubinstein B, Fournier MF, Jacobson K, Verkhovsky AB, Mogilner A (2009). Actin-myosin viscoelastic flow in the keratocyte lamellipod. Biophys J 97, 1853–1863.
Rubinstein B, Jacobson K, Mogilner A (2005). Multiscale two-dimensional modeling of a motile simple-shaped cell. Multiscale Model Simul 3, 413–439.
Ryan GL, Petroccia HM, Watanabe N, Vavylonis D (2012). Excitable actin dynamics in lamellipodial protrusion and retraction. Biophys J 102, 1493–1502.
Satulovsky J, Lui R, Wang YL (2008). Exploring the control circuit of cell migration by mathematical modeling. Biophys J 94, 3671–3683.
Schwarz US, Gardel ML (2012). United we stand—integrating the actin cytoskeleton and cell-matrix adhesions in cellular mechanotransduction. J Cell Sci 125, 3051–3060.
Shao DY, Levine H, Rappel WJ (2012). Coupling actin flow, adhesion, and morphology in a computational cell motility model. Proc Natl Acad Sci USA 109, 6851–6856.
Shebanova O, Hammer DA (2012). Biochemical and mechanical extracellular matrix properties dictate mammary epithelial cell motility and assembly. Biotechnol J 7, 397–408.
Sheetz MP, Felsenfeld DP, Galbraith CG (1998). Cell migration: regulation of force on extracellular-matrix-integrin complexes. Trends Cell Biol 8, 51–54.
Shemesh T, Bershadsky AD, Kozlov MM (2012). Physical model for self-organization of actin cytoskeleton and adhesion complexes at the cell front. Biophys J 102, 1746–1756.

Small JV, Resch GP (2005). The comings and goings of actin: coupling protrusion and retraction in cell motility. Curr Opin Cell Biol 17, 517–523.
Stachowiak MR, McCall PM, Thoresen T, Balcioglu HE, Kasiewicz L, Gardel ML, O'Shaughnessy B (2012). Self-organization of myosin II in reconstituted actomyosin bundles. Biophys J 103, 1265–1274.
Stroka KM, Aranda-Espinoza H (2009). Neutrophils display biphasic relationship between migration and substrate stiffness. Cell Motil Cytoskeleton 66, 328–341.
Totsukawa G, Wu Y, Sasaki Y, Hartshorne DJ, Yamakita Y, Yamashiro S, Matsumura F (2004). Distinct roles of MLCK and ROCK in the regulation of membrane protrusions and focal adhesion dynamics during cell migration of fibroblasts. J Cell Biol 164, 427–439.
Tsai FC, Meyer T (2012). Ca^{2+} pulses control local cycles of lamellipodia retraction and adhesion along the front of migrating cells. Curr Biol 22, 837–842.
Vicente-Manzanares M, Choi CK, Horwitz AF (2009a). Integrins in cell migration—the actin connection. J Cell Sci 122, 199–206.
Vicente-Manzanares M, Ma X, Adelstein RS, Horwitz AR (2009b). Non-muscle myosin II takes centre stage in cell adhesion and migration. Nat Rev Mol Cell Biol 10, 778–790.
Vicente-Manzanares M, Zareno J, Whitmore L, Choi CK, Horwitz AF (2007). Regulation of protrusion, adhesion dynamics, and polarity by myosins IIA and IIB in migrating cells. J Cell Biol 176, 573–580.
Walcott S, Sun SX (2010). A mechanical model of actin stress fiber formation and substrate elasticity sensing in adherent cells. Proc Natl Acad Sci USA 107, 7757–7762.
Welf ES, Ahmed S, Johnson HE, Melvin AT, Haugh JM (2012). Migrating fibroblasts reorient directionality by a metastable, PI3K-dependent mechanism. J Cell Biol 197, 105–114.
Welf ES, Haugh JM (2010). Stochastic dynamics of membrane protrusion mediated by the DOCK180/Rac pathway in migrating cells. Cell Mol Bioeng 3, 30–39.
Welf ES, Haugh JM (2011). Signaling pathways that control cell migration: models and analysis. Wiley Inerdiscp Rev Syst Biol Med 3, 231–240.
Welf ES, Haugh JM (2012). Stochastic models of cell protrusion arising from spatiotemporal signaling and adhesion dynamics. Methods Cell Biol 110, 223–241.
Wolfenson H, Bershadsky A, Henis YI, Geiger B (2011). Actomyosin-generated tension controls the molecular kinetics of focal adhesions. J Cell Sci 124, 1425–1432.
Wolgemuth CW (2005). Lamellipodial contractions during crawling and spreading. Biophys J 89, 1643–1649.
Xiong Y, Huang CH, Iglesias PA, Devreotes PN (2010). Cells navigate with a local-excitation, global-inhibition-biased excitable network. Proc Natl Acad Sci USA 107, 17079–17086.
Zaman MH, Kamm RD, Matsudaira P, Lauffenburger DA (2005). Computational model for cell migration in three-dimensional matrices. Biophys J 89, 1389–1397.
Zimmermann J, Enculescu M, Falcke M (2010). Leading-edge gel coupling in lamellipodium motion. Phys Rev E 82, 051925.